Received: 5 September 2018 | Revised: 27 November 2018 | Accepted: 6 December 2018

DOI: 10.1002/bio.3606

RESEARCH ARTICLE

WILEY LUMINESCENCE
The Journal of Biological and Chemical Luminescence

A high sensitivity system for luminescence measurement of materials

Adrian A. Finch[1] | Yafang Wang[2] | Peter D. Townsend[3] | Martin Ingle[4]

[1] School of Earth & Environmental Sciences, University of St Andrews, St Andrews, UK

[2] School of Science, China University of Geosciences, Beijing, China

[3] Physics Building, University of Sussex, Brighton, UK

[4] Photek Ltd, St Leonards on Sea, UK

Correspondence
Adrian A. Finch, School of Earth & Environmental Sciences, University of St Andrews, St Andrews, Fife KY16 9AL, UK.
Email: adrian.finch@st-andrews.ac.uk

Funding information
the Fundamental Research Funds for the Central Universities of China, Grant/Award Number: 11205134; Natural Environment Research Council, Grant/Award Number: NE/H002715/1; Beijing Higher Education Young Elite Teacher Project, Grant/Award Number: YETP0640; the National Natural Science Foundation of China, Grant/Award Number: 11205134

Abstract

A unique combined and multi-disciplinary wavelength multiplexed spectrometer is described. It is furnished with high-sensitivity imaging plate detectors, the power to which can be gated to provide time-resolved data. The system is capable of collecting spectrally resolved luminescence data following X-ray excitation [radioluminescence (RL) or X-ray excited optical luminescence (XEOL)], electron irradiation [cathodoluminescence (CL)] and visible light from light emitting diodes (LEDs) [photoluminescence (PL)]. Time-resolved PL and CL data can be collected to provide lifetime estimates with half-lives from microsecond timeframes. There are temperature stages for the high and low temperature experiments providing temperature control from 20 to 673 K. Combining irradiation, time resolved (TR) and TR-PL allows spectrally-resolved thermoluminescence (TL) and optically stimulated luminescence (OSL). The design of two detectors with matched gratings gives optimum sensitivity for the system. Examples which show the advantages and multi-use of the spectrometer are listed. Potential future experiments involving lifetime analysis as a function of irradiation, dose and temperature plus pump-probe experiments are discussed.

KEYWORDS

cathodoluminescence, luminescence instrumentation, luminescence lifetime, photoluminescence, radioluminescence, thermoluminescence, time-resolved spectroscopy, X-ray excited optical luminescence

1 | INTRODUCTION

Luminescence offers one of the most sensitive routes to understand the distortions and imperfections in insulating and semiconducting solids. The method benefits from the fact that emission spectra, temperature dependence and excited state lifetimes all differ, providing not only characterization of different types of defect, but also evidence for distortions and clustering in the local environment of those structures. Additionally, luminescence can be excited by a wide range of energetic methods, from site selective photon excitation [photoluminescence (PL)[1]], surface techniques with low energy electrons [cathodoluminescence (CL)[2]] to bulk ionization methods using X-rays [either termed radioluminescence (RL) or X-ray excited optical luminescence (XEOL)[3]] or particle irradiation [ionoluminescence (IL) or ion beam luminescence (IBL)[4]]. Furthermore, one can selectively release charge from particular defect sites after irradiation as a function of temperature, thus providing the site specific information encoded in thermoluminescence (TL).[5,6]

Modern optical detectors with high sensitivity and very low background noise levels mean that responses from impurity or defect sites can be detected well below parts per million (ppm) concentrations. Luminescence spectroscopies are therefore a particularly valuable family of techniques to characterize defect structures in materials, even at low concentrations. Because of the applicability of luminescence across disciplines, the relevant literature is spread across many sciences including condensed matter physics, radiation dosimetry, chemistry, geology, geography and archaeology.[7] The only caveat is that, because of the diversity of applications and user expertise, not all the literature reports data that have been consistently or correctly processed and this may generate apparent differences that are

artefacts of the experimental and data processing methods.[7] With such a wide range of luminescence methods and extreme sensitivity to the target material, it is essential to make several types of measurement on a single sample to understand fully the information encoded in luminescence data. Consequently, one requires a system which has programmable temperature control from e.g. 20 to 673 K, and that can apply all the excitation methods to excite PL, CL, RL and TL. Note also that previous systems often are only capable of ramping the temperature upwards, as for TL, but controlled cooling is equally valuable since it can separate contributions of TL from ramped CL/RL/PL and also reveal hysteresis and single event phase transitions (see literature[8] for example). For some methods either steady state or modulated excitations are required, and from the latter we extract lifetime as well as emission spectral data.

The purpose of this article is to describe a unique luminescence system designed to address these technical and instrumental challenges. The current system has been developed from a system built by Luff and Townsend[9] built in the 1990s which has been substantially upgraded. Its detectors provide state-of-the-art photon sensitivity combined with fast gating of the power to allow time-resolved (TR) spectroscopies. The instrument measures several types of luminescence spectroscopy, including simultaneous multiple excitation, in both continuous wave and pulsed excitation modes as a function of temperature from 20 to 673 K. We illustrate the capabilities of the system with novel data from a selection of industrially relevant materials. We also outline potential future applications.

2 | DESIGN OF THE SYSTEM

2.1 | Introduction

In the early 1990s a system dedicated to the measurement of TL was designed with detection of wavelength multiplexed luminescence made possible by the use of photon imaging detectors[9] and housed at the University of Sussex (Brighton, UK).

On the retirement of Townsend, the system was brought to St Andrews, where new detector systems were installed, several improvements were made and new software was written. There is now a need to describe the modified system with its enhanced sensitivity and greater capabilities. We provide here a description in its current state, without differentiating between the original design and our subsequent modifications.[9]

2.2 | The sample chamber, light path and stages

The system comprises a central chamber made out of aluminium (typically 3 cm thick) and brass (millimetre thick) to reduce X-ray leakage (Figure 1). A USB webcam inside the chamber allows visualization of the sample on the stage. A two-stage vacuum system roughs down to 10^{-1} mbar (10 Pa) with an Edwards Rotary Pump and harder vacuum down to 10^{-6} mbar (0.1 mPa) using a Edwards 100/300 650 W Diffstak diffusion pump. The vacuum status is monitored using Edwards VSK1B vacuum switches and two Edwards APG100 active pirani gauge heads. The vacuum switches close when the vacuum is below a threshold (typically 10 mbar = 1 kPa) and the active vacuum heads provide output voltages between 0 and 6 V as an exponential function of vacuum. These voltages are monitored using a Velleman K8055 USB Experimental Interface board (http://www.velleman.eu/products/view/?country=be&lang=en&id=351346) and converted to an estimate of vacuum – the digital input channels are connected to the vacuum switches and other microswitches around the instrument.

The two-stage vacuum system is controlled by switching mains power on and off to the pumps (rotary and diffusion pumps) using a Measurement Computing USB-ERB08 Electromechanical Relay Interface (http://www.mccdaq.com/usb-data-acquisition/USB-ERB08.aspx). The ERB08 unit also operates the helium compressor, controls venting of the sample chamber during sample change and the safety interlock on the X-ray generator. The stage mounted is detected using microswitches and the program then automatically communicates with the appropriate stage. The system is interlocked for radiation safety and protection of the detectors.

To cover the entire spectrum from ultraviolet (UV) to infrared (IR), two detectors operate simultaneously, targeting the UV-blue and visible-near infrared (NIR) regions, referred to as the 'blue' and 'red' detectors, respectively. Each is housed in separate detector housings, either side of the chamber (Figure 1). The light from the sample is focussed by two sets of two fused silica ('Spectrosil B') plano-convex lenses, a combination which provides 1:1 imaging of the sample on

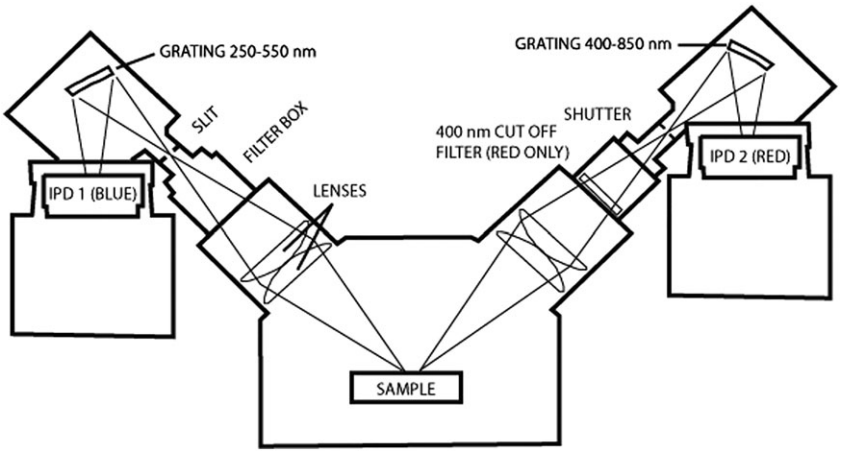

FIGURE 1 Schematic of the luminescence system chamber and detector arrangement. Detection is via two separate detector housings, which cover the region 250–550 nm ('blue detector') and 400–850 nm ('red detector'). The light paths to each detector are slightly different to make sure that each is focussed onto the imaging plate detector (IPD). Excitation of the sample comes from the top. The lenses, filter boxes, shutters and slits are common to both detectors but only labelled on one side for clarity. The 400 nm long pass filter is present only on the 'red' detector

the entrance slits of the spectrometers. The lenses seal directly to the sample chamber, eliminating the need for additional windows in the sides of the chamber. In the case of the 'UV-blue' detector (see later), fused silica elements are necessary to enable UV transmission, but a further advantage of this material is its good resistance to radiation darkening. Since the lenses receive a considerable dose over time from scattered radiation in the chamber, fused silica is used for both lens combinations, even in the 'red' detector where UV is not measured. Lens combinations, rather than single lenses, are necessary to match the high f number of the spectrometers ($f/2.2$). Between the lenses and the entrance slits are lightproof boxes that accept standard (50 mm × 50 mm) filters. The entrance slits to the spectrometers can be swapped to modify the signal strength and spectral resolution, but the typical analysis takes place with 500 µm slits providing a typical wavelength precision of approximately 2 nm but widths of 125, 250 and 1000 µm are available. Manual shutters are placed in the light paths after the filter boxes.

The focal position of the spectrum is a function of wavelength, and hence the distances from the sample to each detector are different, optimized for the central wavelength region that each detector analyses.[9] The light is diffracted by American Holographic Chemspec 100S concave gratings of the flat-field holographic type; one is used nominally for the range 200–450 nm (ref: 446.02/L) with a dispersion of 8 nm/mm and the other (ref: 446.14/L) from 400 to 800 nm with a dispersion of 12 nm/mm. The numerical aperture is $f/2.2$. The peak efficiency of each grating occurs at approximately 350 and 730 nm, chosen near the centre of each spectral range, biased to enhance signals where the red photocathode sensitivity is falling steeply.

Second-order scattering of lower wavelengths into the first-order spectrum will occur for the red grating detector, therefore a GG400 Schott Glass 400 nm long pass filter is permanently inserted into the light path of the red detector to remove the short wavelength signals (Figure 1). The filter is not entirely opaque between 397 and 400 nm and for samples with a strong signal in this region, we observe a small second-order response between 795 and 800 nm. Rather than attempt difficult corrections for this artefact, we accept that this remains in processed spectra of samples that are strong in the UV-blue. The two detectors provide two separate sets of spectral data with a substantial overlap from which subsequent data processing creates a single composite UV-IR spectrum.

The chamber is furnished with two heating stages for cryogenic (20–300 K) and high-temperature (300–673 K) measurement. A third heating stage operating from −40 to +400°C is also available for samples which have TL transitions around room temperature. The cryostage enters from below the chamber and the high temperature stage at the front; each has a blanking plate to isolate the chamber when the other stage is in use. The low temperature stage is a Cryophysics M22 cryostage, cooled by a CTI Cryogenics 8200 water-cooled Helium Compressor and heated with nichrome wire. Temperature is controlled by a Eurotherm 2404 controller connected to a Au-Fe thermocouple. The maximum ramp rate is 0.1 K/s. The cryostage is operated only when the sample has been in vacuum ($<10^{-5}$ mbar = <1 mPa) for some hours, to avoid frosting of the sample. The higher temperature heating stages have a Nichrome strip 12 mm × 50 mm × 0.7 mm and a chromel/alumel thermocouple controlled by a Eurotherm 818P controller with switching accomplished by a Eurotherm thyristor unit model 462. The maximum ramp rate of the high temperature stage is 3 K/s.

2.3 | The detectors

The diffraction gratings deliver a strip of light onto the detector, such that the position of the photon arrival is a function of wavelength. The detectors are imaging plate detectors (IPDs) manufactured to our specifications by Photek Ltd (www.photek.co.uk). IPDs were chosen to provide state-of-the-art sensitivity whilst also allowing sub-microsecond switching of the power to the detector plate for TR luminescence experiments (see later). Cooled detectors were not favoured to avoid frosting of the detector – the difficulties associated with keeping the detector under vacuum or dry nitrogen were considered to overwhelm the benefits of lower dark current. IPDs use standard photomultiplier tube (PMT) photocathode materials; however, electron multiplication is provided by microchannel plates (MCPs) rather than a dynode chain. Charge clouds emerging from the channels are proximity focussed onto a resistive anode. The current flow resulting from the original photon event is measured at four points on the resistive anode, enabling the position of the photon arrival and its arrival time to be reconstructed. Each IPD has a separate power unit and communicates to the master computer via USB. The 'blue' detector is a bialkali photocathode IPD; the 'red' detector is a S25 based photocathode – each detector type was chosen to maximize signal and minimize noise in the relevant spectral range. The dark current on each detector was typically 2.4×10^{-4} (blue) and 1.6×10^{-2} Hz nm^{-1} (red) but we observe a halo effect such that the dark current is lower in the centre and enhanced towards the edges. This foreshortening of the image was ameliorated against by an optional software patch. A fuller description of the imaging plate detectors is given in Supporting Information S1. The position on the IPD is calibrated against wavelength using Hg, Kr emission lines and laser pointer sources and the output from the detectors are both raw images and reconstructed wavelength. Blackbody radiation in the IR is seen as a background in all runs using the high-temperature stage above approximately 600 K and becomes progressively more intense as temperature rises to the maximum (673 K).

The system and detectors used here exploit the high sensitivity and dynamic range of photocathode detectors. However, they have a weakness in that their performance falls at long wavelengths. By contrast one can use a charge coupled device (CCD) signal collection which functions into the NIR region. Our system has sufficient access ports that in principle it is simple to add a fibre optic link to a longer wavelength CCD spectrometer for those materials which require such data. We have used CCD systems successfully during the recording of ion beam excited luminescence[10] and synchrotron-based XEOL.[11]

2.4 | Sample excitation

Three forms of excitation are available: (1) a Philips MCN-101 ceramic X-ray tube placed at the rear of the chamber; (2) an electron gun (taken from a JEOL electron microscope) on the top; (3) light emitting

diodes (LEDs) inserted inside the chamber and controlled by power sources externally. The X-ray and electron gun sources were controlled manually by units in the electronic rack. The X-ray controller is not operated above 30 kV and 15 mA to avoid X-ray leakage; typical operating conditions are 20 kV and 4 mA, providing dose rates of 1.8 Gy/min measured in quartz. The electron gun operates between 10 and 25 kV acceleration voltage with a typical beam current of 200 nA and a spot size typically with a diameter of 3 mm, providing an incident power density of approximately 1 kW/m^2. The beam is focussed using the electron optics inherited from the electron microscope source, controlled by external power supplies. Beam position (x–y) is tweaked using external magnetic fields generated by solenoids controlled by power supplies; beam pulsing is achieved by sudden increases in the current applied to these, flipping the beam off the sample. Typical switch speeds are in the microsecond range and typical repetition rates are 1 ms (but this is changed to explore different lifetimes). The LEDs are sourced either from RadioSpares (uk.rs-online.com) or Roithner LaserTechnik GmbH (www.roithner-laser.com) and controlled via an amplifier built in-house and operated by a logic signal to be either on or off. Emission wavelengths down to 300 nm have been used although deeper UV LEDs are now available. Continuous wave PL is difficult since the excitation would saturate the sensitive detector plates. PL is achieved with the use of notch or long pass filters, or by exciting in the UV and only using data from the visible-NIR detector. TR-PL is achieved without the use of filters by less than a millisecond switching of the LEDs coupled to rapid switching of the detectors.

2.5 | System software

Software was written in-house using LabVIEW 2016 (www.ni.com/labview/) to operate from a Graphical User Interface (GUI). All automated components of the system are controlled by LabVIEW drivers but some were provided in other languages (e.g. visual basic or C) and adapted using LabVIEW wrappers. LabVIEW drivers for the stages are downloaded from National Instruments and adapted for the present system. The Eurotherm 818 controller (high temperature stage) uses a version of an older 808 driver by enabling extra commands compatible with the 818. The Eurotherm 2404 controller (low temperature heating stage) is successfully operated via a generic 2400 series driver. Both controllers work via RS232 protocol, operated via USB using a 4-way USB-RS232 converter.

The detectors come with Photek software (Image 32) which can be operated directly or controlled from LabVIEW using wrappers provided by Photek. Photon arrivals are accumulated over preset integration periods, assigning a position on the imaging plate and a time stamp to every photon arrival. The output is a 16-bit monochrome image covering the entire detector area. Photon arrival events outside the rectangular area illuminated by the grating are rejected. Direct image transfer from the Photek software to LabVIEW results in the loss of the most significant bit in the data, and hence the program writes the image data to the hard drive from Image 32 and reads it back into LabVIEW as a 16-bit image using routines in the LabVIEW Image Module. For continuous wave (CW) measurements, the time stamps are ignored and the two-dimensional image from each detector is converted to a one-dimensional spectrum by summing individual pixel values onto the wavelength axis.

For time resolved (TR) analysis, excitation is pulsed and photon arrivals in the 'off' cycle are analysed as a function of wavelength and arrival time. Since the power to the IPD is switched off during this cycle, TR-PL or optically stimulated luminescence (TR-OSL) is possible without any filters since the intense light from the LED arrays do not encounter the detector whilst the voltage is on, thereby avoiding damage to the detector. If the energy of excitation is above that of the measured luminescence, the process is PL but the present system allows energies higher than those of the irradiation to be measured (i.e. OSL). TR analysis uses LED (TR-PL) or electron beam excitation (TR-CL). The electron beam is pulsed by flicking the beam off the sample using an electromagnet on the column; LEDs are controlled by pulsing the power to them. We observe approximately 1 μs phosphorescence from some cheaper LEDs after the power is stopped. Although more expensive nano-LEDs with rapid fall characteristics are available, we have found it more convenient to use cheap LEDs and insert a software delay (typically 3 μs) between the end of the 'on' excitation signal and powering up the detectors. Blank measurements with the delay show no sign of the primary excitation in TR-PL. Photon arrival times during data acquisition are binned over multiple iterations producing a 16-bit rectangular image with wavelength on one axis and numbers of photons per time bin on the other. Time bin widths are software controlled but are typically 250 ns, 200 bins and integration times of 5 min provide data that we have processed successfully (see later) to provide estimates of lifetime in the microsecond to second range.

Longer (seconds to hour length) lifetimes are measured using a 'phosphorescence' routine in LabVIEW whereby repeated CW spectra are collected and then amalgamated to create a two-dimensional image. The outputs from this type of analysis emulate those of TR analysis so that the same software routines are applied.

2.6 | Offline data processing and manipulation

We store data as raw files and system corrections are performed offline. This allows alternative system corrections and data manipulation to be performed retrospectively without the need to reconstruct raw images. We have preferred this approach particularly since offline processing software is regularly improved. The data from the individual detectors are corrected first by subtracting the dark current (as a function of wavelength and exposure time), then dividing by the system responses of the two IPDs (Figure 2, provided by Photek). We also correct the data for grating efficiency which amplifies the deeper UV data and improves the fitting of the two spectra (R^2 are increased, see later). The effects of the transmission of the quartz lenses (and the 400 nm long pass filter in the red detector) are also accommodated. The two spectra are matched in the overlapping spectral region, typically 420–480 nm, avoiding the edge regions of both spectrometers where the dark current is high and image foreshortening is observed. Because of the steric effects of the sample and different focus distances to the two imaging plates, the amount of light arriving at the two detectors is never perfectly matched in intensity. We scale the two images with

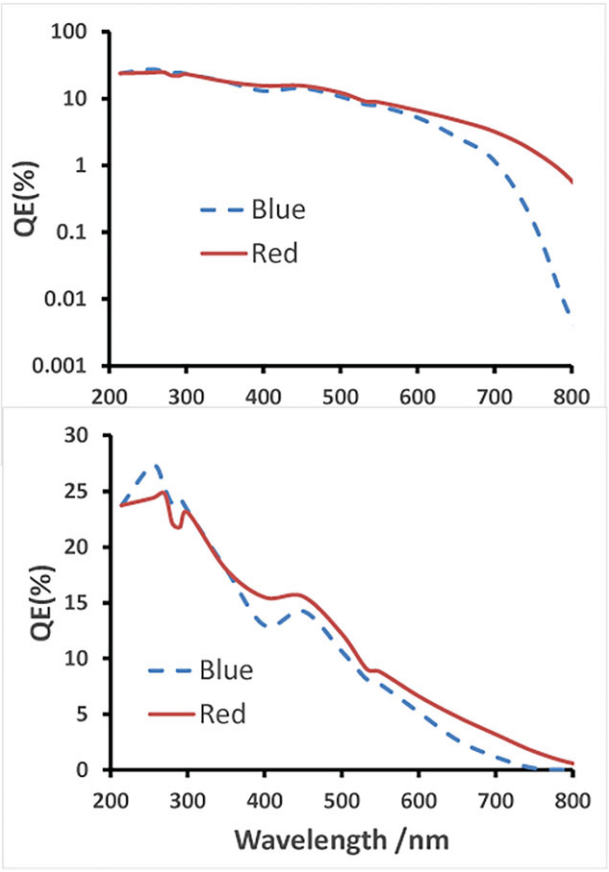

FIGURE 2 Relative quantum efficiencies (QEs) of the imaging plate detectors (IPDs). The UV-blue detector is shown as a dashed blue line and the 'red' detector as a solid red line. Data are shown on both log and linear *y*-axis scales so that the relative efficiencies in the visible and the infrared (IR) can both be understood. The bialkali IPD used on the UV-blue detector has better performance in the UV, whereas the S25 detector has better performance in the visible and IR

respect to each other to accommodate, with the overlap region comprising a linear combination of the two images. We calculate a fit index (R^2) to express how the two images match with linear scaling. Where significant signal is present, R^2 values > 95% are observed. Analysis of single emission band profiles in energy space give Gaussian fits, suggesting that our system corrections provide accurate and undistorted final profiles. At temperatures above 600 K (approximately 320°C), significant blackbody radiation is observed in the spectra at 800 nm which increases and creeps to shorter wavelengths with increasing temperature. The blackbody radiation from the stage is often many orders of magnitude greater that the luminescence signals from the samples, hence the data for the high temperature stage are deleted where significant blackbody radiation occurs in a sample blank.

The final outputs are transferred automatically to ORIGIN for plotting and standard three-dimensional (3D) and contour plots (used in the present study) are generated automatically. These are typically contoured with 'hot' colours to express higher counts and 'cold' colours as lower ones (e.g. Figures 3 and 4). However, in recognition of the many in the science community who are colour blind (including one of us), the software also generates monochrome contour-based outputs which we present in Supporting Information S2. Examples of

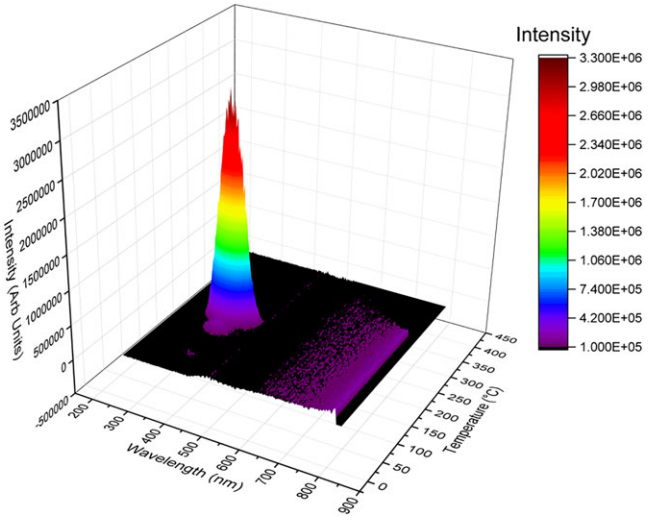

FIGURE 3 High temperature thermoluminescence (TL) of LiF:Mg,Cu,P (GR200) dosimeter material expressed as a three-dimensional (3D) graph. Data are system corrected and the region of the spectrum where significant blackbody radiation is observed (above 320°C at 800 nm and moving diagonally across the graph) has been deleted. The strong TL emission centred at 381 nm and 188°C is clearly visible

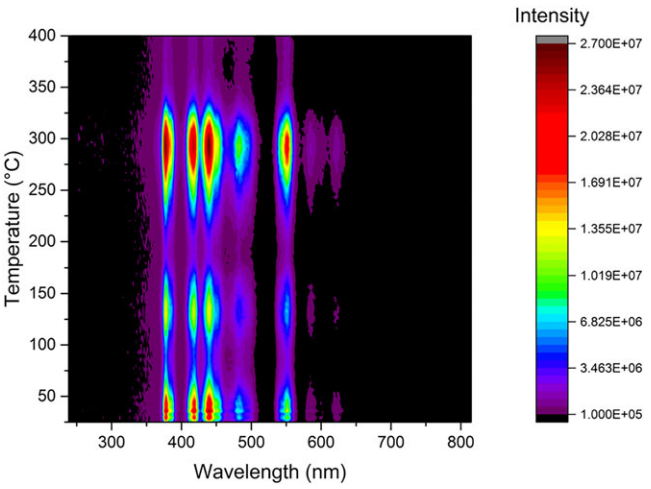

FIGURE 4 High temperature thermoluminescence (TL) of Mg_2SiO_4:Tb expressed as a contour plot. Terbium (Tb) emissions at 376, 417, 438, 483, 550, 586 and 621 nm are observed and TL glow peaks occur at 35, 133 and 293°C. Black and white alternatives to this colour format are available in the Supporting Information

the raw and processed data formats are attached to the present article as Supporting Information S3.

3 | EXAMPLES OF LUMINESCENCE DATA

We present data here from a cross-section of materials designed to explore and test the accuracy and capabilities of the system. We have used both well-characterized samples, whose data can be related to the open literature, and a selection of more challenging materials which provide novel observations and provide insights into the future capabilities of the system and the types of scientific questions that this system might address. Data are collected using both the high temperature and cryogenic stages.

3.1 | TL and dosimeter materials

GR200 is doped LiF:Cu,Mg,P and is one of the most commonly used dosimeters for the personal radiation dosimetry. High temperature TL data for GR200 were collected in the temperature range from 20 to 400°C after 2 Gy X-irradiation (Figure 3). In order to minimize temperature gradients across the sample, a heating rate of 0.1 K/s is usually employed. In this example, the TL of the sample occurs at 188°C with a wavelength maximum at 381 nm. As can be seen from Figure 3, the TL of this material is particularly effective dosimeter material using conventional TL (spectrally unresolved) since its peak emission in the blue/near UV is close to the optimum quantum efficiency of a PMT (typically about 400 nm).

Figure 4 shows a 3D plot of TL from a $MgSiO_4$:Tb dosimeter material.[12] The terbium (Tb) emission lines are dominant and extend across the UV and visible. The irradiation was 100 Gy and the heating rate was 0.25 K/s over the temperature range from 25 to 400°C. We observe emissions at 379, 417, 440, 483, 550, 583 and 621 nm (consistent with the published spectrum of McAllister[13]) and maxima at 35, 133 and 293°C. This material is a particularly useful test since the spectrum is the product of the two separate detectors and are 'stitched' together to provide a single spectrum. The wavelengths of the example demonstrate that not only can the system readily resolve the Tb emission lines, but also the data obtained from the two separate detector units are successively resolved into a single spectrum. The wavelength peaks are consistently within a few nanometres of the expected values, the reported accuracy of the spectrum.

Figures 3 and 4 show that TL can be readily observed, not only providing the glow peak temperature, but also spectral resolution (cf. Wang et al.[14]). We readily observe TL in less sensitive dosimeter materials, including alumina,[15] quartz, feldspar and sodalite.[16] We improve signal-to-noise in the least sensitive materials by increasing the initial dose (longer X-irradiation times) and/or the temperature ramp rate. Faster ramp rates produce more photons per second, and therefore a better signal-to-noise for weak signals, although a discrepancy between the temperatures of the sample and the thermocouple may be evident at the highest ramp rates.

Figure 5 shows the low temperature TL of pink sodalite ($Na_8Al_6Si_6O_{24}Cl_2$). The data show four glow peaks at 66, 105, 190 and 232 K. However, the 66 and 232 K TL peaks occur at 690 nm whereas the 105 and 190 K peaks predominantly lie in the UV and blue (309 and 411 nm) regions. The spectroscopic resolution of the system allows the shift in the wavelength of the TL to be observed, something that is absent from conventional spectrally-unresolved TL. This material is discussed further later.

3.2 | XEOL and phosphors

The X-irradiation delivers photons with energies equivalent to the binding energies of core electrons. Hence, X-irradiation liberates electrons and the subsequent luminescence (XEOL or RL) derives from energy cascades as electrons fall into the empty core electron states. To explore the efficacy of the system at measuring XEOL, we present data for a natural sodalite. XEOL often provides relatively bright signals compared to TL. Each pixel on the detector plate has a maximum bin depth of two^{16} counts, and bright samples saturate the bins. Furthermore,

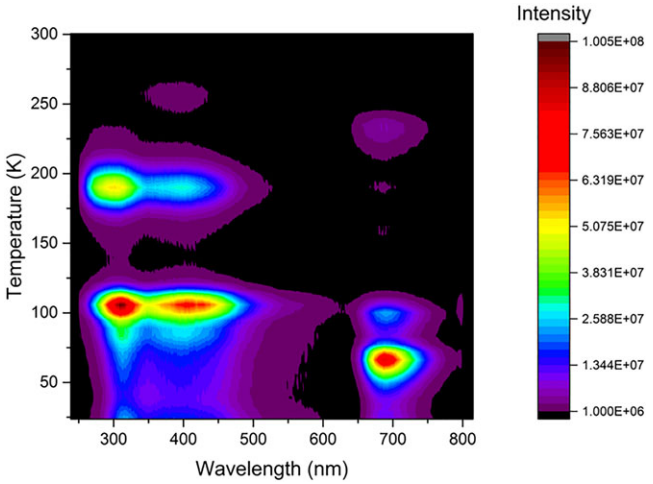

FIGURE 5 Low temperature thermoluminescence (TL) of pink sodalite (AF-07-35) as a contour map. Data are system corrected and expressed as arbitrary intensity using the colour scheme on the right. A variety of TL glow peaks are observed at 66, 105, 190 and 232 K, whose responses occur at different wavelengths. The 66 and 232 K TL peaks occur at 690 nm whereas the 105 and 190 K peaks predominantly occur in the UV and blue (309 and 411 nm)

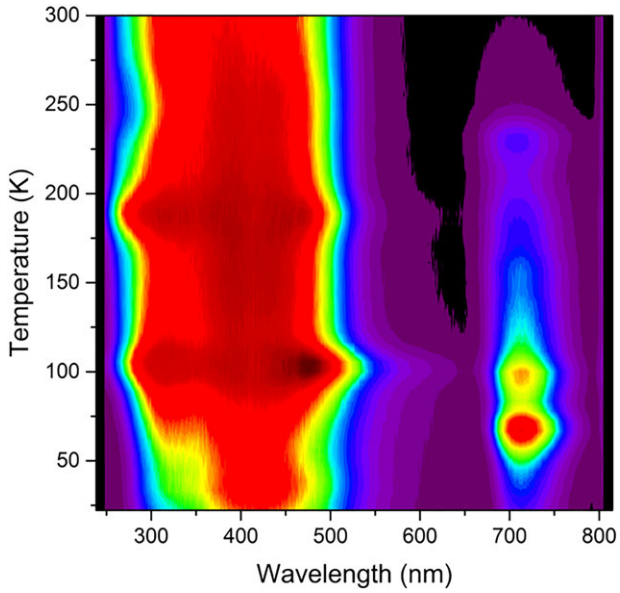

FIGURE 6 X-ray excited optical luminescence (XEOL) and thermoluminescence (TL) composite data from pink sodalite (AF-07-35). Where fast ramp rates are employed, XEOL data from the instrument are composites of XEOL and TL. The small peaks in intensity (particularly evident at 690 nm and 66 K) are TL responses (Figure 4) added to the XEOL, better called the XEOLTL response. The true isolated XEOL can be achieved by slowing ramp rates down substantially (although this increases the acquisition times and the data density), or by taking the spectra on the cooling cycle

very fast accumulation is associated with non-linearity in the relationship between counts and brightness and the very brightest signals trip the internal protection software for the detector, switching the power to the detectors off. For these reasons, brighter materials are accommodated by reducing integration times (making sure individual pixels in the image do not saturate) and/or light attenuation including (a)

smaller slits before the gratings and/or (b) the use of pinholes and neutral density filters. Normally we repeat experiments which have used the highest bit of any pixel on the image.

For dimmer materials, we integrate for longer, and increase the slit width before the gratings, accepting that this results in a loss of wavelength resolution. The system is normally operated with 500 μm slits but these can be opened to 1000 μm, broadly increasing the signal four-times. Dimmer materials such as poorly responsive diamond, quartz and feldspar have been successfully measured on the system, but here we present novel data for the framework silicate sodalite.[16] XEOL data can be obtained as a function of temperature and incident power (e.g.Wang et al.[17]). The XEOL as a function of temperature of a pink sodalite (AF-07-35) is presented in Figure 6. This shows a strong broad band in UV-blue with a less intense peak in the red-NIR. A feature of the data are notable peaks in the red-NIR band at 66 and 105 K and localized broadening of the UV-blue band at 105 and 190 K, observed as a stripe across the data at that temperature. Comparison of the XEOL of the sample (Figure 6) with the TL (Figure 4) show that these features correspond to TL peaks in the sodalite. The XEOL data are collected at a relatively fast ramp rate (0.1 K/s) to allow the spectrum to be collected in a convenient timeframe. However, with continuously increasing temperature, the data produced are actually a composite of the XEOL and TL behaviour, which we call 'XEOLTL'. Normally we infer the isolated XEOL behind the TL without further experimentation, but the TL contribution to the data can be diminished by (a) slowing the temperature ramp rate, (b) inserting pauses at each temperature before the light is measured or (c) measuring the XEOL during the cooling cycle.

The sodalite data are of particular interest, since the 66 and 232 K TL occur in the red-NIR region (Figure 4), whereas XEOL at the same temperature is dominated by the UV-blue emission (Figure 6). We interpret this to indicate that there is coupling of the trap (in both energy and spatial senses) and the recombination site. Observations such as this provide not only direct evidence for the coupling of electron traps and recombination centres, but also potentially insights into the physical nature of traps in dosimeter materials.

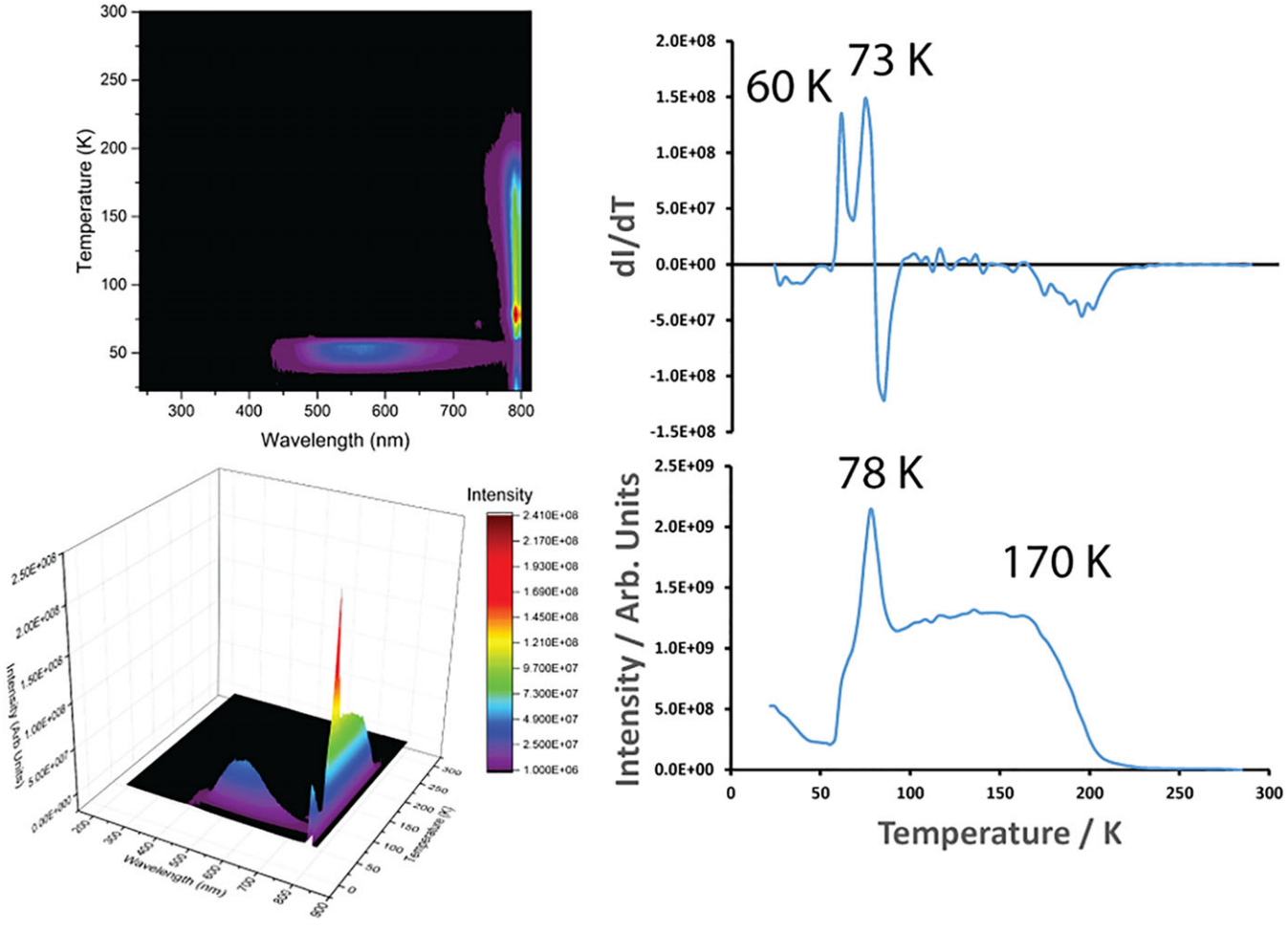

FIGURE 7 X-ray excited optical luminescence (XEOL) data from $SrTiO_3$ at 15 kV and 4 mA X-generation. The same data are shown as a three-dimensional (3D) graph (top left) and a contour plot (bottom left). The near-infrared (NIR) emission at approximately 794 nm is close to the wavelength limit of the system and the long wavelength part of the emission is truncated. The temperature dependence of the NIR band is shown bottom right. The intense broad band centred at 568 nm has a sharp maximum at 54 K whereas the NIR band at 794 nm has sharp peaks at 24 and 78 K and a minimum at 54 K – precisely the temperature at which the 568 nm band is strongest. The very sudden loss of the orange band on warming to 60 K and the intense NIR band which peaks at 78 K encompass the temperature of a phase transition in $SrTiO_3$ which is expressed very clearly in the data. Phase transitions are often particularly evidence in the first derivative of the data (top right) and we infer the two peaks in the first derivatives define different stages of the phase transition

3.3 | Structural phase changes

Luminescence data have long been used to study imperfections and to characterize lattice distortions since the signals are sensitive to changes of structure (particularly point symmetry) and composition. Previous work has included intentionally added probe ions, such as lanthanides, to sense distortions in local crystal fields caused by modified structural environments. An underexploited extension of this approach is to use luminescence to monitor crystalline phase changes. Figure 7 shows XEOL of a $SrTiO_3$ crystal from 20 to 300 K with the heating rate of 0.1 K/s.[17] Very strong changes in wavelength and intensity of the luminescence accompany the region between 50 and 80 K, the temperature window in which $SrTiO_3$ undergoes phase transitions.[18] The temperature profile of the NIR emission shows a maximum at 78 K and a point of inflexion in intensity at 180 K (Figure 7). We also show the first derivative of those data with respect to temperature (dI/dT). Phase transition temperatures are most closely approximated by maxima in the first derivatives of intensity – here the transition appears as a two stage process with a maximum at 73 K, within a few kelvin of the published inversion temperature (70 K).

Phase transitions are often associated with strong TL, and we have designed the system so that contrasts in luminescence lifetime can also be explored. All of these methods are sensitive probes of structural state in which phase transitions are particularly evident.

3.4 | PL and luminescence lifetime measurement

The instrument measures light emitted from X- or electron-irradiation in continuous mode, i.e. the excitation and detectors are on simultaneously. PL can be measured in CW mode by closing off one of the detectors (e.g. the UV-blue) and exciting in that range, whilst measuring the response in the visible-NIR spectrometer, or by the use of notch filters. However, thanks to fast switching of the power to the detectors and by pulsing the laser diodes, the light emitted from the sample is measured while the laser diode is in the 'off' cycle. No filters are necessary and the spectra measured can include the wavelength of the excitation. The acquisition rates of the detectors are such that only luminescence with lifetimes in microseconds or longer can be measured. The data can be acquired as a single spectrum, providing a single snapshot of the luminescence spectrum a few microseconds after the commencement of the off cycle. Such data are useful where light intensities are poor and merely an impression of the longer (> 1 μs) lifetime components of a PL spectrum is sufficient. However, it is usually more informative to collect multiple time slices from the spectra, providing a 3D graph comprising wavelength (x), time (y) and light intensity (z) which can be expressed in either contour or 3D graphical formats (Figure 8). Intensities are system corrected so that different parts of the spectrum can be directly compared. The instrument set-up allows different lifetimes to be measured simultaneously in different parts of the spectrum. For example, the TR luminescence at 145 K of a $CaSO_4$:Tm,Li phosphor has been studied using PL excitation with 460 nm LEDs (Figure 8). The decay of Tm^{3+} luminescence is clear, resulting from the Tm^{3+}: $^1G_4 \rightarrow {}^3H_6$, $^1G_4 \rightarrow {}^3F_4$ and $^3F_3 \rightarrow {}^3H_6$ transitions whose wavelengths are at 477, 655 and 698 nm, respectively.[19] Visual analysis of the graph shows the presence of a broad band around 620 nm and the Tm^{3+}: $^3F_3 \rightarrow {}^3H_6$ doublet at 698 nm that are constant through the timeframe of the experiment. Time slices can

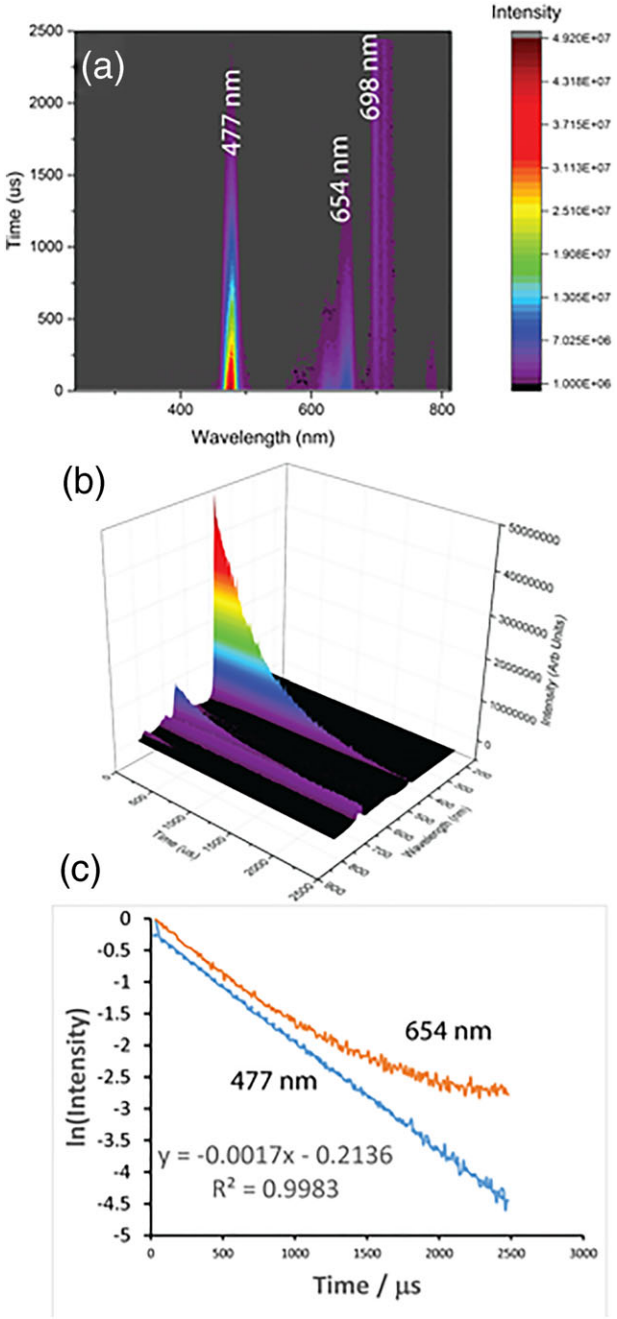

FIGURE 8 Time-resolved photoluminescence (PL) of $CaSO_4$:Tm,li at 155 K. The luminescence intensity as a function of temperature and wavelength is shown in contour (a) and three-dimensional (3D) graph formats (b). The decay of the emissions as a function of time is clear for particularly the 477 and 654 nm emissions. A broad emission between 698 and 710 nm is essentially constant over the lifetime of the experiment. The decay profiles of the 477 and 654 nm emissions are fitted in (c). The blue component fits a single exponential decay (R^2 = 0.998) whose slope corresponds to a decay half-life of 582 ± 3 μs; the orange band is initially consistent with this lifetime but the flattening of the data as time increases indicates an additional, longer lifetime component. The intensity of the 697–710 nm region is essentially constant throughout the experiment, showing its half-life is > > 5 ms

be extracted from the data and modelled to provide estimates of decay lifetimes (Figure 8c). The half-life of the blue emission is consistent with a single exponential decay lifetime (τ) of 582 ± 3 μs. Lifetimes in the millisecond range are commonly reported for f–f transitions within Tb^{3+} (e.g. Kroon et al.[20]), although this can be reduced by coupling the local environment, particularly interlanthanide energy transfer (e.g. Padlyak and Drzewiecki[21]). The orange emission comprises two components, one of which is long (> 2.5 ms) and the other is similar to the lifetime of the blue emission (Figure 8c). The key point is that the system can resolve in a single session the lifetimes of all the emissions in the spectra range and provide independent lifetime estimates.

4 | FUTURE DIRECTIONS

The new system is designed to allow novel luminescence experiments to be performed. Earlier data have shown that the signals generated by PL, CL or RL independently not only offer different spectra (as expected) but, when two excitation sources are combined, the resultant signal is not the sum of the two separate processes (our unpublished data). The opportunities for these more subtle probes have now been implemented in the layout of the experimental sample chamber, including pump-probe experiments where one excitation is continuous and another is pulsed. Such experiments explore, for example, the luminescence of excited states. The software currently collects the data from one cycle (either 'off' or 'on') and protects the detector by switching the power off for the other. A pump-probe experiment can be achieved by two separate configurations, each measuring the 'off' and 'on' cycles separately, so long as the excitation is invisible to the detector (by stimulating in e.g. the IR or by exciting in the UV and switching the UV-blue detector off). In such an experiment, there is no reason why the detector could not remain on for both cycles, but binning the data separately such that the responses of both off and on cycles are provided as independent images. This would allow data from both cycles to be collected simultaneously in a single experimental run. Although the existing software is currently not configured to allow this, Photek have indicated that such an upgrade is relatively easy.

The TR capabilities of the system open a wide range of PL spectroscopies. Triplet states with wavelengths similar to those of the excitation can be measured (normally long pass filters remove data close to the excitation wavelength) and we can compare and contrast in real time direct excitation (where the luminescence is measured at energies below excitation) with stimulation and upconversion (which are slow, i.e. less than microsecond lifetimes and where the spectrum is analysed at energies above the energy of the incident light). Spectrally resolved OSL – a spectrally resolved variant of a widely used method in retrospective dosimetry – has been achieved.

The ability to quantify spectra in the time domain allows luminescence lifetime to become a parameter in the characterization of our materials. Our current methods for analysing TR data are manual and automated analysis is necessary to analyse larger volumes of data. Fitting of spectra as surfaces is being developed, so that fluorescence emissions which overlap in both lifetime and wavelength can be resolved. Such data will be important in separating the competing luminescence from e.g. the same ion on non-equivalent crystallographic sites. In addition, where the wavelength of the emission is consistent with one emission band, but analysis of lifetime indicates both fast and slow components, this may indicate coupling of the luminescence centre with a non-radiative defect (i.e. Förster resonance). Such data provide insights into e.g. defect clustering and the distribution of ions over non-equivalent sites. Experiments which include analysis of wavelength, lifetime, temperature and light intensity create substantial four-dimensional datasets, which require data reduction to be readily understandable. We are developing software to allow lifetimes to be extracted automatically from such data and then compared from one run to the next as a function of temperature, exploring the dependence of lifetime and wavelength on temperature. We have no doubt that the flexibility of the system will allow other experiment types to be achieved.

ACKNOWLEDGEMENTS

The authors would like to thank the support of the Fundamental Research Funds for the Central Universities of China, the National Science Foundation of China (No.11205134) and Beijing Higher Education Young Elite Teacher Project (YETP0640). The refurbishment of the RLTLCL system at St Andrews was funded by NERC grant NE/H002715/1.

ORCID

Adrian A. Finch https://orcid.org/0000-0002-3689-1517
Yafang Wang https://orcid.org/0000-0002-9988-5034

REFERENCES

[1] H. Friis, A. A. Finch, C. T. Williams, J. M. Hanchar, *Phys. Chem. Miner.* **2010**, *37*, 333.
[2] P. D. Townsend, A. P. Rowlands, Information encoded in cathodoluminescence spectra, in *Cathodoluminescence in Geosciences*, (Eds: M. Pagel, V. Barbin, P. Blanc, D. Ohnenstetter), Springer, Berlin **2000** 41.
[3] H. Friis, A. A. Finch, C. T. Williams, *Phys. Chem. Miner.* **2011**, *38*, 45.
[4] A. A. Finch, D. Hole, P. D. Townsend, J. Garcia-Guinea, J. M. Hanchar, *J. Phys. D Appl. Phys.* **2004**, *37*, 2795.
[5] B. Yang, P. D. Townsend, A. P. Rowlands, *Phys. Rev. B* **1998**, *57*, 178.
[6] T. Karali, N. Can, P. D. Townsend, A. P. Rowlands, J. Hanchar, *Am. Mineral.* **2000**, *85*, 668.
[7] Y. Wang, P. D. Townsend, *JOL* **2013**, *142*, 202.
[8] B. Yang, P. D. Townsend, *J. Mod. Opt.* **2001**, *48*, 319.
[9] B. J. Luff, P. D. Townsend, *Meas. Sci. Technol.* **1993**, *4*, 65.
[10] P. D. Townsend, *Nucl. Inst. Methods B* **2012**, *286*, 35.
[11] R. P. Taylor, A. A. Finch, J. F. W. Mosselmans, P. D. Quinn, *JOL* **2013**, *134*, 49.
[12] H. Tarawa, M. Masukawa, A. Nagamatsu, K. Kitajo, H. Kumagai, N. Yasuda, *Radiat. Meas.* **2011**, *46*, 709.
[13] W. A. McAllister, *J. Electrochem. Soc.* **1966**, *113*, 226.
[14] Y. Wang, Y. Zhao, D. White, A. A. Finch, P. D. Townsend, *JOL* **2017**, *184*, 55.
[15] M. L. Chithambo, A. N. Nyirenda, A. A. Finch, N. S. Rawat, *Phys. B* **2015**, *473*, 62.

[16] A. A. Finch, H. Friis, M. Maghrabi, *Phys. Chem. Miner.* **2016**, *43*, 481.

[17] Y. Wang, Y. Zhao, Z. Zhang, C. Zhao, X. Wu, A. A. Finch, P. D. Townsend, *JOL* **2015**, *166*, 17.

[18] T. Hasegawa, M. Shirai, K. Tanaka, *JOL* **2000**, *87-89*, 1217.

[19] N. K. Giri, A. K. Singh, D. K. Rai, S. B. Rai, *Opt. Commun.* **2008**, *281*, 3547.

[20] R. E. Kroon, H. C. Swart, O. M. Ntwaeaborwa, H. A. A. Seed Ahmed, *Phys. B* **2014**, *439*, 83.

[21] B. Padlyak, A. Drzewiecki, *J. Non Cryst. Solids* **2013**, *367*, 58.

SUPPORTING INFORMATION

Additional supporting information may be found online in the Supporting Information section at the end of the article.

How to cite this article: Finch AA, Wang Y, Townsend PD, Ingle M. A high sensitivity system for luminescence measurement of materials. *Luminescence*. 2019;34:280–289. https://doi.org/10.1002/bio.3606